Biosensors and Bioelectronics 272 (2025) 117134

Contents lists available at ScienceDirect

Biosensors and Bioelectronics

journal homepage: www.elsevier.com/locate/bios

# An off-chip platform for on-demand, single-target encapsulation for ultrasensitive biomarker detection

Yuxin Zhang [a], Jiahao Zheng [a], Bayinqiaoge [b], Tim Cole [a], Chengchen Zhang [b,**], Yi Wang [a,***], Shi-Yang Tang [a,b,c,*]

[a] Department of Electronic, Electrical and Systems Engineering, University of Birmingham, Edgbaston, Birmingham, B15 2TT, UK
[b] School of Electronics and Computer Science, University of Southampton, Southampton, SO17 1BJ, UK
[c] School of Mechanical and Manufacturing Engineering, University of New South Wales, Sydney, NSW, 2052, Australia

ARTICLE INFO

*Keywords:*
Microdroplets
ddELISA
Off-chip
Microfluidics
Biosensing

ABSTRACT

Closed-channel microfluidic systems offer versatile on-chip capabilities for bioanalysis but often face complex fabrication and operational challenges. In contrast, free-boundary off-chip microfluidic platforms are relatively simple to fabricate and operate but lack the ability to perform complex tasks such as on-demand single-target sorting and encapsulation. To address these challenges, we develop an off-chip platform powered by a fluorescent-activated mechanical droplet sorting and production (FAM-DSP) system. The system integrates target detection, sorting, encapsulation, and on-demand droplet generation into a single compact platform, eliminating the need for microfabrication and minimizing the use of specialized fluidic control equipment. It achieves precise single-target encapsulation with a high efficiency of over 70%. Such a capability is applied for improving the performance of droplet digital enzyme-linked immunosorbent assay (ddELISA) by reducing the number of empty droplets and increasing the throughput, enabling precise quantification of target biomarkers with a low limit of detection. This versatile off-chip platform holds promise not only for biomarker detection but also for single-cell analysis and various applications in clinical diagnostics and biomedical research.

## 1. Introduction

Droplet microfluidics has revolutionized the field of single-cell and single-molecule analysis by allowing precise control over the microenvironment in which biochemical reactions occur (Moragues et al., 2023; Sánchez Barea et al., 2019; Joensson and Andersson Svahn, 2012). Traditional microfluidic systems rely on microchip-based approaches, where microchannels are used to guide fluid flow (Nielsen et al., 2020). These systems have been instrumental in the development of various high-throughput assays, including the droplet digital enzyme-linked immunosorbent assay (ddELISA), which enables the detection of low-abundance protein-based biomarkers with high sensitivity (Cohen et al., 2020; Cohen and Walt, 2017). However, microchip-based platforms often face limitations such as complex fabrication processes inside a cleanroom, the need for sophisticated fluid control equipment, and difficulties in scaling up for high-throughput applications (Nielsen et al., 2020; Zhu et al., 2024). Off-chip platforms, particularly those utilizing free-boundary droplet generation, have emerged as a promising alternative. These platforms simplify the droplet generation process by eliminating the need for intricate microchannels, instead relying on the natural formation of droplets at the interface between immiscible fluids (Zhu et al., 2024; Ye et al., 2022; Zhang et al., 2020; Tang et al., 2019).

Recent advancements in droplet microfluidics have focused on enhancing the efficiency of droplet generation and the specificity of sorting methods. Techniques such as air-assist (Zheng et al., 2023; Zhang et al., 2021) and dielectrophoretic (Zhang et al., 2023; Zhang and Abate, 2020; Cole et al., 2017) sorting have been developed to improve the precision and throughput of droplet assays. These methods leverage external forces to manipulate droplets, ensuring that only those containing targets are retained for analysis, thereby reducing the number of empty droplets and increasing the efficiency of single-cell and single-molecule studies (Collins et al., 2015; Kaminski et al., 2016). Although the air and dielectrophoretic sorting methods are powerful, they require relatively bulky and costly systems to operate, such as

* Corresponding author. School of Mechanical and Manufacturing Engineering, University of New South Wales, Sydney, NSW, 2052, Australia.
** Corresponding author.
*** Corresponding author.
*E-mail addresses:* chengchen.zhang@soton.ac.uk (C. Zhang), Y.Wang.1@bham.ac.uk (Y. Wang), shiyang.tang2@unsw.edu.au (S.-Y. Tang).

https://doi.org/10.1016/j.bios.2025.117134
Received 29 September 2024; Received in revised form 30 November 2024; Accepted 3 January 2025
Available online 4 January 2025

high-pressure gas control systems with digital pneumatic valves or high-voltage pulse generation modules. Additionally, other on-chip approaches without applying external forces, such as the bead-ordered arrangement droplet (BOAD) system, have demonstrated significant reductions in empty droplets through pre-focusing and ordering mechanisms, achieving single-bead encapsulation efficiencies as high as 86% (Yue et al., 2022). Despite these advancements, strategies for on-demand encapsulation in off-chip systems remain significantly underexplored.

In ddELISA, samples are partitioned into a large number of discrete droplets, each acting as an independent reaction chamber (Guan et al., 2014; Shim et al., 2013). This partitioning allows for the amplification and detection of target molecules in a digital format, where each droplet is scored as either positive or negative for the presence of the target. Microbeads play a crucial role in ddELISA by enabling the capture, detection, and quantification of low-abundance target biomolecules with high precision. The encapsulation of individual target-carrying microbeads within picolitre microdroplets minimizes target dilution and enhances detection sensitivity (Cohen et al., 2020; Yi et al., 2022; Yelleswarapu et al., 2019). The use of microbeads makes droplet sorting significant for ddELISA. During droplet production, samples need to be diluted for single-bead encapsulation, resulting in a large number of empty droplets. Since ddELISA often relies on image-based analysis to detect droplets with fluorescent signals, the presence of many empty droplets makes this process time-consuming due to the need to process a large number of images, thereby hindering throughput improvement. Therefore, by employing droplet sorting techniques, such as fluorescence-activated sorting, ddELISA platforms can selectively isolate droplets containing microbeads, further improving assay performance. However, achieving on-demand encapsulation in off-chip systems remains challenging due to the difficulties in controlling droplet formation and sorting in a free-boundary environment.

In this work, we address the above-mentioned challenges by developing a versatile off-chip microdroplet production platform for on-demand, single-bead encapsulation. This platform is powered by an integrated fluorescent-activated mechanical droplet sorting and production (FAM-DSP) system. The FAM-DSP system is compact and low-cost, integrating both sorting and droplet production functionalities. The precise target encapsulation is achieved through the synchronization of real-time fluorescence detection and mechanical actuation for droplet production. The FAM-DSP system enables significant improvements in the performance of ddELISA, particularly in reducing the number of empty droplets and increasing the throughput of single-target encapsulation. The ability to produce uniformly sized microdroplets with precise control over their size and composition, coupled with high-throughput sorting and droplet production mechanisms, lays the foundation for further advancements in off-chip droplet microfluidics. This platform has potential applications extending beyond biomarker detection to single-cell analysis and other areas of clinical diagnostics and biomedical research (Mazutis et al., 2013; Kaushik et al., 2018).

## 2. Experimental section

*Chemicals, Instruments, and Fabrication:* Span®80 surfactant, mineral oil, Tween®20, Phosphate buffered saline (PBS), EDC (N-(3-Dimethylaminopropyl)-N′-ethylcarbodiimide hydrochloride) Bovine Serum Albumin (BSA), Sulfo-NHS (N-Hydroxysulfosuccinimide sodium salt), OptiPrep™ density gradient medium, MES and Rhodamine 6G were purchased from Sigma-Aldrich. fluorescein di-β-d-galactopyranoside (FDG), Streptavidin-β-galactosidase (SβG) and dyed red aqueous fluorescent particles (R0100) were purchased from Thermo Fisher Scientific. Glass puller was used for applicability modification. A tube revolver rotator (Fisher Scientific) was used in all incubation processes. For the construction of the platform, a small solenoid actuator (12 V, 30 mm × 10 mm × 11 mm), and glass capillary were purchased from eBay. The frames, glass capillary holder, fibre alinement structures and microtube holder in the beaker were fabricated using a fused deposition modelling (Ultimaker S5) and a stereolithography 3D printer (Formlabs Form 3). A syringe pump (PHD, 2000; Harvard Apparatus) was used to inject the solutions into the platform. A high-speed camera (CHRONOS 1.4, Kron Technologies Inc.) was used to capture the high-speed videos.

*Fibre Optic Detection Unit:* Fiber Buffer Stripper (Thorlabs), Ruby Scribe (S90R, Thorlabs), and Fiber Grippers (BFG1, Thorlabs) were used in manual optic fibre cleaving. A 532 nm laser module (100 mW) was used as the fluorescent excitation light source. Other components for the optic fibre detection system include a photomultiplier tube (PMT1001, Thorlabs), two fibre port collimators (PAF2P-11A), short-pass dichroic mirror (DMSP550R), dichroic mirror cage (CM1-DCH), and optic fibres (M146L02-Ø400 μm and M122L02-Ø200 μm) were purchased from Thorlabs. A multifunctional digital data acquisition module (USB 6001, National Instruments) was used for collecting signals generated by the photomultiplier tube and triggering the actuation of the solenoid.

*Preparation of Antibody Coated Capture Beads:* Capture antibodies for interferon-gamma (IFN-γ, PeproTech 500-M90) were reconstituted and stored according to the manufacturer's instructions. The IFN-γ capture antibody was diluted to 0.5 mg/mL in the Coupling Buffer (0.05 M MES buffer, pH 5.0) and stored on ice until ready for use. Around $2.8 \times 10^8$ superparamagnetic fluorescent, carboxyl-functionalized beads (PS-MAG-Fluo-COOH, 4.54 μm, microParticles GmbH) were transferred into a microtube and washed three times with 200 μL of the Coupling Buffer. The beads were centrifuged at 12,000 rpm for 3 min between each wash, then placed on a magnetic separator to prevent disruption, and the supernatant was discarded. Fresh solutions of 50 mg/mL EDC and 50 mg/mL Sulfo-NHS were prepared in the Coupling Buffer. Then, 20 μL of Sulfo-NHS solution and 20 μL of EDC solution were added to the beads, and the mixture was vortexed for 5 s. The beads were incubated for 20 min at room temperature with the tube revolver rotator. Following incubation, the beads were centrifuged at 12,000 rpm for 3 min and the supernatant was discarded. The beads were then resuspended in 400 μL of the Coupling Buffer. This wash step was repeated two more times, and the beads were finally resuspended in 180 μL of the Coupling Buffer.

An appropriate volume of capture antibody (approximately 20 μL) was added to the activated beads and mixed by vortexing for 5 s. The mixture was incubated for 2 h at room temperature using a tube revolver rotator. After incubation, the beads were centrifuged at 12,000 rpm for 3 min, then placed on a magnetic separator to prevent disruption, and the supernatant was discarded. The capture antibody-conjugated beads were then washed twice with 200 μL of the Coupling Buffer. The beads were resuspended in 200 μL of the Blocking Buffer (PBS containing up to 1% BSA, pH 7.4) and placed on the rotator for 1 h to block any remaining non-specific binding sites. The beads were centrifuged at 12,000 rpm for 3 min and the supernatant was discarded. Then, the beads were resuspended in 200 μL of the Storage Buffer (PBS containing 0.01% Tween® 20, 0.05% $NaN_3$, and 0.1% BSA, pH 7.4). The beads were stored at 4 °C.

*Preparation of Reagents and Immunoassay Assay Setup:* Capture antibody-coated beads were diluted in PBS buffer. A total of ~100,000 beads per sample were used for the ddELISA assay. Biotinylated detection antibodies (R&D Systems BAF285) were diluted in PBS buffer to the concentration of 0.2 μg/mL. SβG stock solution was reconstituted and stored according to the manufacturer's instructions. SβG solution was diluted in PBS buffer to 50 pM. Recombinant protein standards (R&D Systems 285-IF) were serially diluted to the desired concentration in PBS buffer. In a two-step assay configuration, 25 μL of bead suspension, 100 μL of sample, and 20 μL of detector antibody were pipetted into a microtube and incubated for 2 h. The beads were then pelleted with a magnet, and the supernatant was removed. Following several washes, 100 μL of SβG was added and incubated for 10 min. After the last wash, the beads were resuspended in 100 μL of the substrate solution, which consists of 85 μL of 100 μM FDG (fluorescein di-β-d-galactopyranoside) and 15 μL of OptiPrep™. The bead suspension was thoroughly mixed using a pipette and then loaded into the encapsulation device for partitioning into droplets.

## 3. Results and discussion

Fig. 1 presents the workflow and components of the FAM-DSP system (see Fig. S1 for the actual setup). Fig. 1a illustrates the fluorescent-activated target encapsulation process, where the aqueous phase containing fluorescent targets is pumped into a glass capillary (inner diameter of 100 μm) and directed into a container with an immiscible oil (mineral oil) phase containing surfactant (2% Span®80) necessary for droplet generation. The outlet of the glass capillary is submerged a few millimetres under the oil surface, allowing the aqueous phase to form droplets due to interfacial tension, gravity, and shear forces. The droplets then sink to the bottom of the oil phase and empty droplets are considered wastes. As the fluorescent targets pass through the detection section, a laser-coupled optical fibre induces fluorescent signal emission from the targets, and the emission signal is collected by the detection system *via* an optical fibre placed outside the transparent glass capillary. When the target approaches the glass capillary tip (inner diameter of 15 μm), the actuator is triggered by the detection module's upstream signal, allowing the target to flow out and form target-laden microdroplets, which are then collected in a separate compartment (a 200 μL microtube) placed within the glass beaker for further experiments.

Fig. 1b details the integrated sorting and target-encapsulation system, which features a 3D-printed frame housing essential components including the mechanical solenoid actuator, glass capillary, glass capillary holder, and optical fibre alignment structures. The solenoid actuator controls the precise movements of the capillary tip, ensuring consistent droplet formation. Additionally, the microtube holder securely positions the microtubes, while the beaker contains the oil phase for droplet generation. A closer view of the fibre optic detection unit is provided in Fig. 1c. This setup includes an excitation source and emission collection fibres aligned at the thin neck of the glass capillary. The excitation source fibre (green) is a multimode fibre with a 200 μm diameter, while the emission collection fibre (red) is a multimode fibre with a larger diameter (400 μm), ensuring sufficient fluorescent emission signal capture. An optical-quality end face is achieved by manually cleaving the fibres using a ruby scribe. The cleaved optical fibres are inserted into the 3D-printed supporting structure to ensure accurate alignment and direct contact with the outer surface of the glass capillary. The thin neck structure of the glass capillary is fabricated using a micropipette puller, with parameters such as heating intensity, heating time, and puller displacement set to elongate the capillary without breaking, resulting in a thin neck with an inner diameter reduced from 100 μm to 50 μm. This allows the target to flow through the optic detection area, preventing the bead signal from deviating from the fibre's detection region caused by a relatively large-sized off-chip capillary setup. In addition, an index-matching gel was used at the contact section at the tip of the optic fibre, minimizing the fluorescent signal loss. This precise alignment is vital for accurate optical measurements,

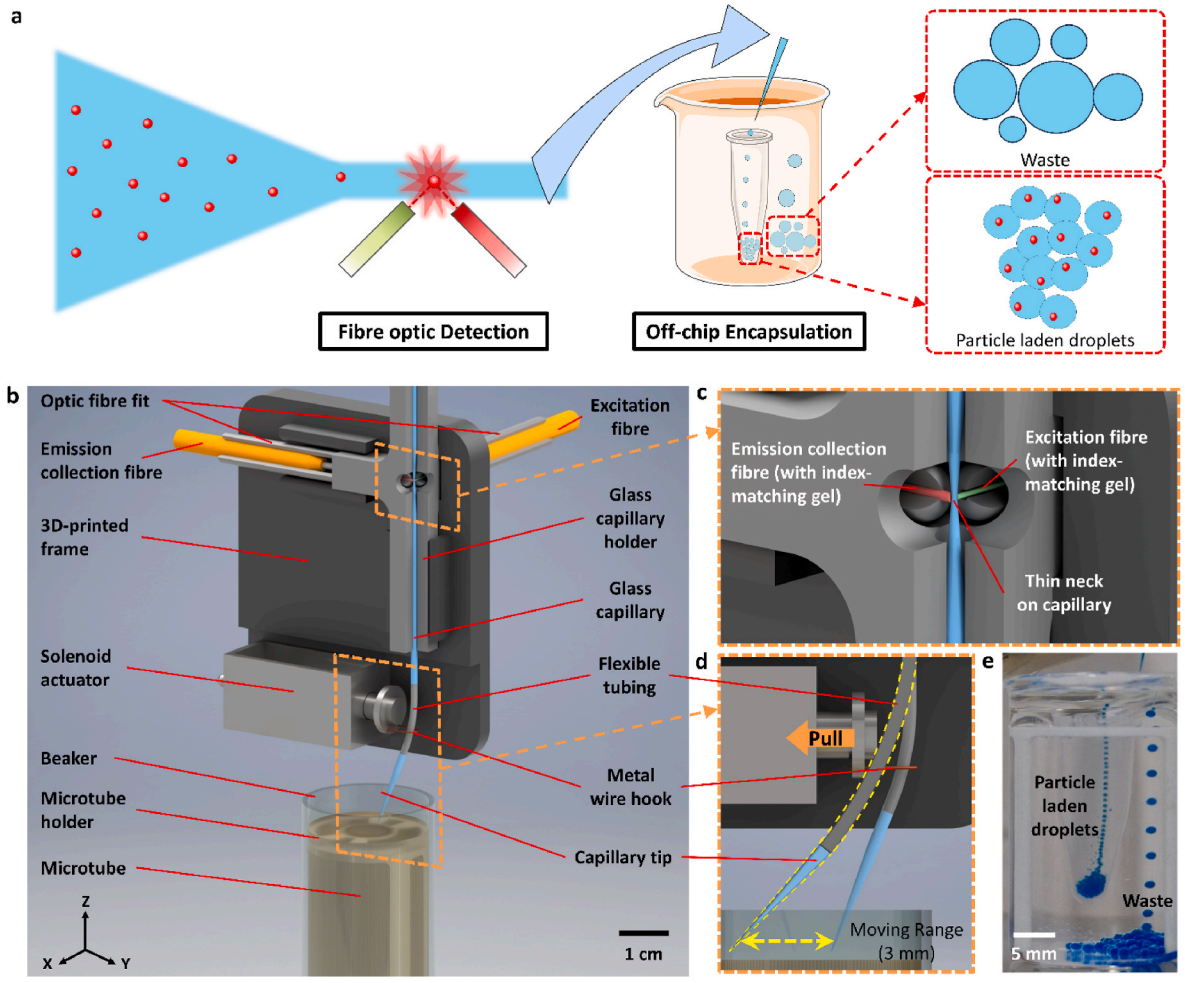


**Fig. 1.** Schematic and working principles of the FAM-DSP system. a) Schematic drawing of the fluorescent-activated target sorting and encapsulation processes. b) Schematic representation of the off-chip sorting and target-encapsulation system. c) Zoomed-in schematic of the fibre optic detection unit setup. d) Zoomed-in schematic of the mechanical actuator-enabled off-chip encapsulation unit and the moving principle. e) Demonstration of on-demand microdroplet generation in the oil phase with fixed holding time. The aqueous phase is mixed with blue food dye for better visibility. (For interpretation of the references to colour in this figure legend, the reader is referred to the Web version of this article.)

allowing real-time detection of fluorescence signals from the encapsulated targets within the droplets. The solenoid actuator is triggered based on signals generated by the optical fibre detection unit, ensuring the generation of microdroplets that contain the target.

Fig. 1d zooms in on the mechanical actuator-enabled off-chip encapsulation unit, highlighting its moving principle. The solenoid actuator controls the position of the capillary tip, which is connected to the glass capillary using a flexible tubing. The flexible tubing is constrained with a metal wire hook, which is connected to the actuator. When the actuator is triggered by the fluorescent detection unit, the hook first pulls the flexible tubing, placing the capillary tip above the microtube for collection. After a certain amount of holding time, the actuator pushes the capillary tip back to its original position. The shear induced by the pushing movement, combined with the droplet's inertia, detaches the droplet from the capillary tip, generating a microdroplet that encapsulates the target. Droplets of different sizes are achieved by controlling the flow rate of the aqueous phase and the holding time of the actuator. The moving range of the capillary tip is 3 mm, and the average moving speed of the capillary tip is 200 mm/s. The slide friction between the metal wire hook and the flexible tubing is reduced by applying lubrication oil, and the shock caused by the actuation is largely absorbed with soft rubber tape placed on the solenoid actuator, allowing for the production of microdroplets with high uniformity. As a demonstration, an actual image of on-demand microdroplet generation with fixed holding time is shown in Fig. 1e. Microdroplets that contain targets can be produced in the oil phase and collected in the microtube, while wasted droplets are formed outside the microtube when no target is detected.

Fig. 2a provides a more detailed illustration of the droplet generation process through a series of sequential snapshots taken from a high-speed camera. In this experiment, the holding time ($T_{hold}$) is set to 400 ms, and the flow rate of the aqueous phase ($Q$) is 1 μL/min (see also Movie S1). The following is the detailed droplet formation process.

1. Initial Stage (0 ms): At the onset of the process, the capillary tip is positioned at the waste side, and the aqueous phase continuously flows out. When the actuator is triggered, it initiates the movement of the capillary tip.
2. Transition Stage (8 ms): The capillary tip moves toward the microtube side. Due to the high moving speed, no aqueous residue remains at the tip.
3. Positioning Stage (15 ms): The capillary tip is pulled above the microtube for droplet collection. The droplet starts to grow as more of the aqueous phase is dispensed into the oil phase.
4. Growth Stage (415 ms): After a holding time of 400 ms, the droplet develops to the desired size. Precise holding time allows the droplet to achieve the appropriate volume before detachment.
5. Detachment Stage (423 ms): The actuator pushes the flexible tubing back, and the induced shear force, along with the droplet's inertia, causes it to detach from the capillary tip. The droplet is then collected by the microtube placed underneath.
6. Return Stage (430 ms): The capillary tip returns to its starting position at the waste side, completing the droplet generation cycle and preparing for the next one.

This set of experiments demonstrates the precision and control achievable in the droplet generation process using the encapsulation unit. By fine-tuning $T_{hold}$ and $Q$, we can consistently produce microdroplets of various sizes that contain the target for subsequent bioanalytical applications.

Due to the large size of the droplet compared to the capillary tip and the rapid movement of the solenoid actuator, the droplet's inertia,

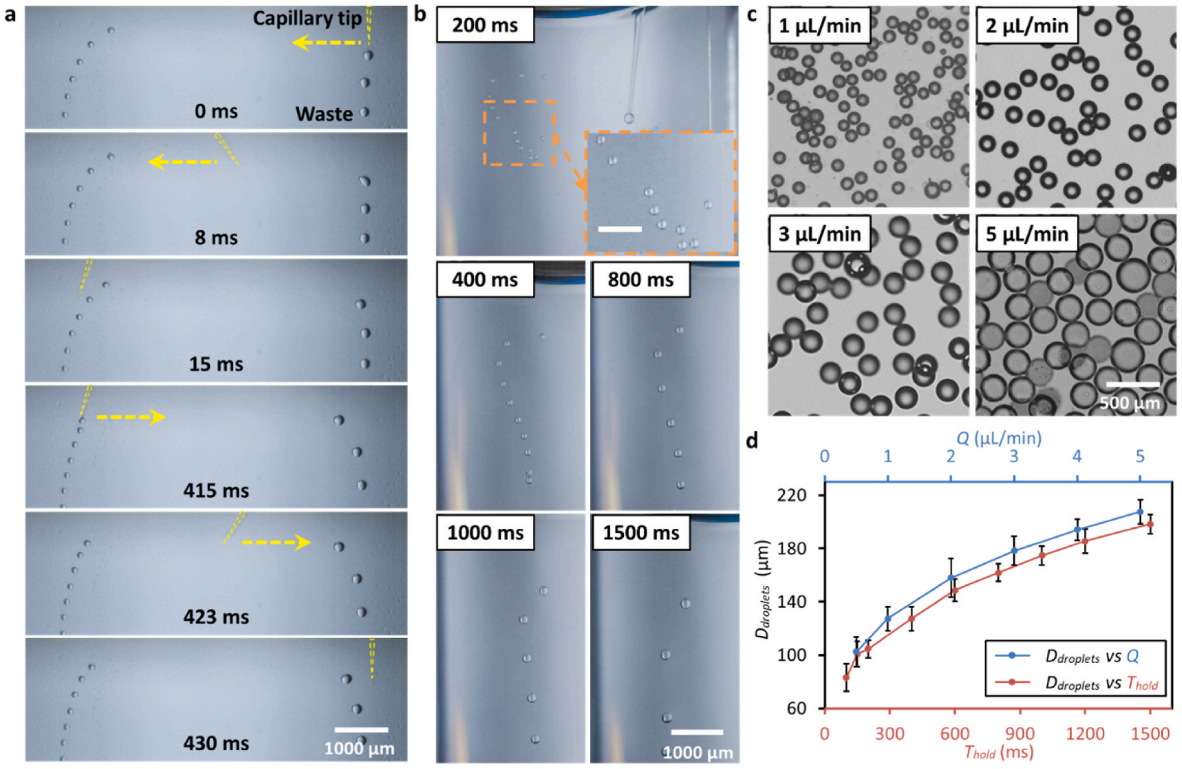


**Fig. 2.** Droplet formation process and controlling the size of the produced microdroplets. a) Sequential snapshots showing the formation of a microdroplet (capillary tip is highlighted in yellow and its moving direction is marked with arrows). b) Snapshots taken from a high-speed camera showing the production of water microdroplets at different $T_{hold}$ of 200, 400, 800, 1000 and 1500 ms. The inset is a magnified image of the produced microdroplets (Scale bar is 500 μm). c) Optical images of the produced water microdroplets at different $Q$ of 1, 2, 3, and 5 μL/min d) Plots of droplet diameter $D_{droplet}$ *vs* $T_{hold}$ or $Q$. (For interpretation of the references to colour in this figure legend, the reader is referred to the Web version of this article.)

rather than the Capillary number, dominates the production process. This is evident in Movie S1, where almost no movement of the produced droplet is observed during the detachment stage. Therefore, the diameter of the droplet ($D_{droplet}$) is proportional to the product of $T_{hold}$ and $Q$, as given by:

$$D_{droplet} \propto T_{hold} \bullet Q \quad (1)$$

Keeping the flow rate $Q$ constant at 4 μL/min, prolonging $T_{hold}$ efficiently increases the size of the produced microdroplets, as shown in Fig. 2b (see also Movie S2). On the other hand, Fig. 2c illustrates that at a constant $T_{hold}$ (400 ms in this case), a higher $Q$ results in the production of droplets with a larger size (see also Movie S2). Fig. 2d summarises the diameter of the produced microdroplets with respect to $T_{hold}$ and $Q$, respectively. The diameter of the produced microdroplet ranges from 80 to 210 μm under different operating conditions, and the coefficient of variation (CV) of the size is less than 7%. The size of the produced droplets is also influenced by the nozzle size of the glass capillary. Using a 15 μm nozzle, our system can effectively generate droplets with diameters as small as ~50 μm.

Durability tests conducted over 2000 cycles confirmed no significant degradation in the solenoid actuator's performance or droplet encapsulation efficiency, demonstrating the FAM-DSP system's reliability for high-throughput applications. As shown in Fig. S2, the system maintained stable performance throughout extended cycles. The actuator's temperature increased from room temperature to a saturated state at 25.3 °C under 12 V and 26.5 °C under 28 V, with no changes in moving speed observed before or after reaching thermal saturation, highlighting the system's robustness. Increasing the operating voltage from 12 V to 30 V effectively enhanced the glass tip's actuating speed from 200 mm/s to approximately 400 mm/s, facilitating higher throughput. However, excessively high voltages may risk damaging the solenoid and the glass tip. Furthermore, at higher actuating speeds, the formation of tiny satellite droplets along the moving range led to increased polydispersity, as shown in Fig. S3.

The FAM-DSP system uses a fibre optic detection unit to generate a triggering signal that determines the production of target-laden droplets. As shown in Fig. 3a, the detection unit consists of a laser (532 nm) as the excitation light source, a dichroic mirror coupled photomultiplier tube (PMT) for fluorescent signal collection, two optical fibres for light transmission, a multifunctional digital data acquisition module, and a computer for signal processing and control. A 200 μm diameter multimode optical fibre guides the excitation light from the laser source. The scattered and emitted light from the targets is collected by a 400 μm optical fibre, which directs the light to a dichroic mirror cage. The filtered fluorescent emission signal is then transmitted to the PMT. Two fibre port collimators are used in the laser and the dichroic mirror cage to collimate the excitation and emission signals, focusing the light signal to ensure high sensitivity. This fibre optic detection module in the FAM-DSP system demonstrates reliable detection of fluorescent targets, with sufficient sensitivity to identify fluorescent microparticles. To further assess the sensitivity, we test the system with a range of fluorophore samples, including 1 μm microparticles and Rhodamine 6G at different concentrations (Fig. S4). These tests validate the high sensitivity of our system across a broad dynamic range, ensuring reliable detection even with varying signal intensities.

A multifunction I/O device is used as the data acquisition system and outputs actuator-triggering signals. Fig. 3b demonstrates examples of PMT, filtered, and triggering signals for detecting and encapsulating fluorescent microbeads. The signals are processed, analysed, and generated using LabVIEW. The dichroic mirror coupled PMT measures the intensity of the fluorescent light emitted by a microbead, converting it into electrical voltage signals corresponding to the detected peaks. The PMT signal (Galvo-Galvo scanner and bandwidth was set at 250 kHz) is then transmitted to the PC, where it is first denoised with a low-pass filter (Butterworth filter, cutoff frequency: 100 Hz, order: 2) and then analysed. When a peak is detected and the magnitude is above the

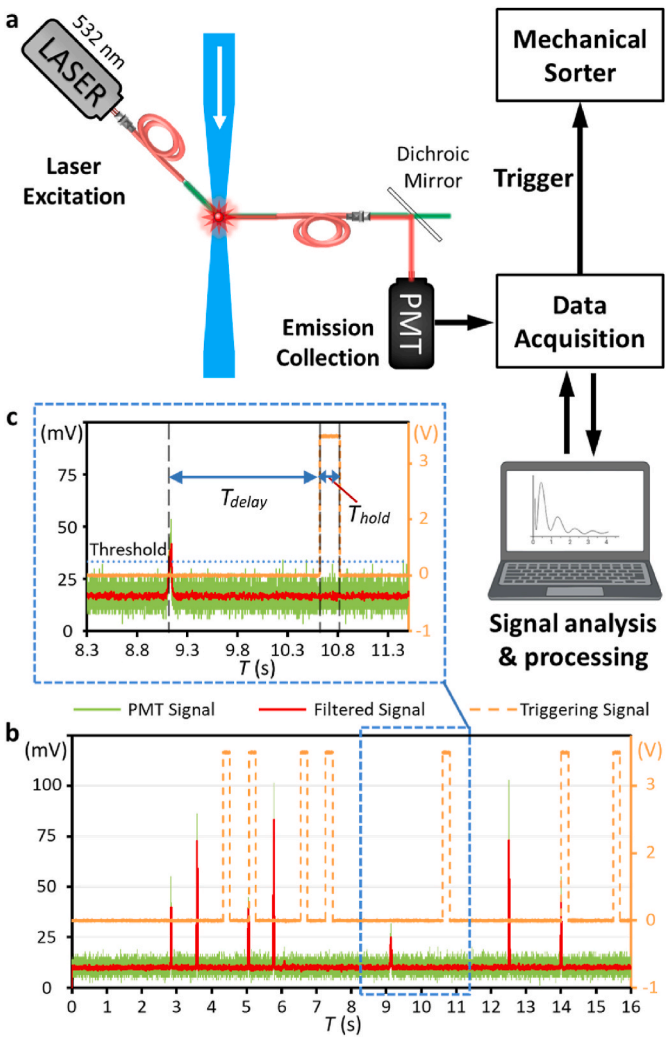


**Fig. 3.** Configuration of the fibre optic detection unit. a) The unit consists of a laser module, a dichroic mirror coupled PMT, two optic fibres, a data acquisition module, and a computer. b-c) Examples of the PMT signal, the filtered signal, and the triggering signal for controlling the actuator.

threshold, a triggering signal is generated and sent to the driving circuit (see Fig. S5 for the circuit design) of the mechanical actuation system. As shown in Fig. 3c, a delay time ($T_{delay}$) is needed to allow the particle to approach the capillary tip, and a holding time ($T_{hold}$) is necessary to allow the droplet to grow for determining the droplet size. $T_{delay}$ is determined for different flow rates and adjusted based on experimental results, while $T_{hold}$ can be adjusted for different droplet size requirements. The processed signals are continuously monitored and displayed on a PC, allowing real-time analysis of the detected microbead. Threshold levels are set to differentiate between background noise and actual particle detection events.

In the absence of a sorting mechanism, the rate of single-bead encapsulation within droplets can be predicted using the Poisson distribution (Collins et al., 2015). This statistical approach assumes that microbeads are randomly distributed in the fluid medium and that the droplet formation process occurs at a constant flow rate. When no sorting is applied, the bead-laden distribution primarily follows the Poisson distribution, resulting in a significant proportion of droplets being empty or containing multiple beads, thus leading to inefficient encapsulation and increased variability (Collins et al., 2015; Liu et al., 2020). The implementation of the FAM-DSP system, as evidenced by Fig. 4, greatly reduces the number of empty droplets.

This enhancement is particularly notable when comparing the before

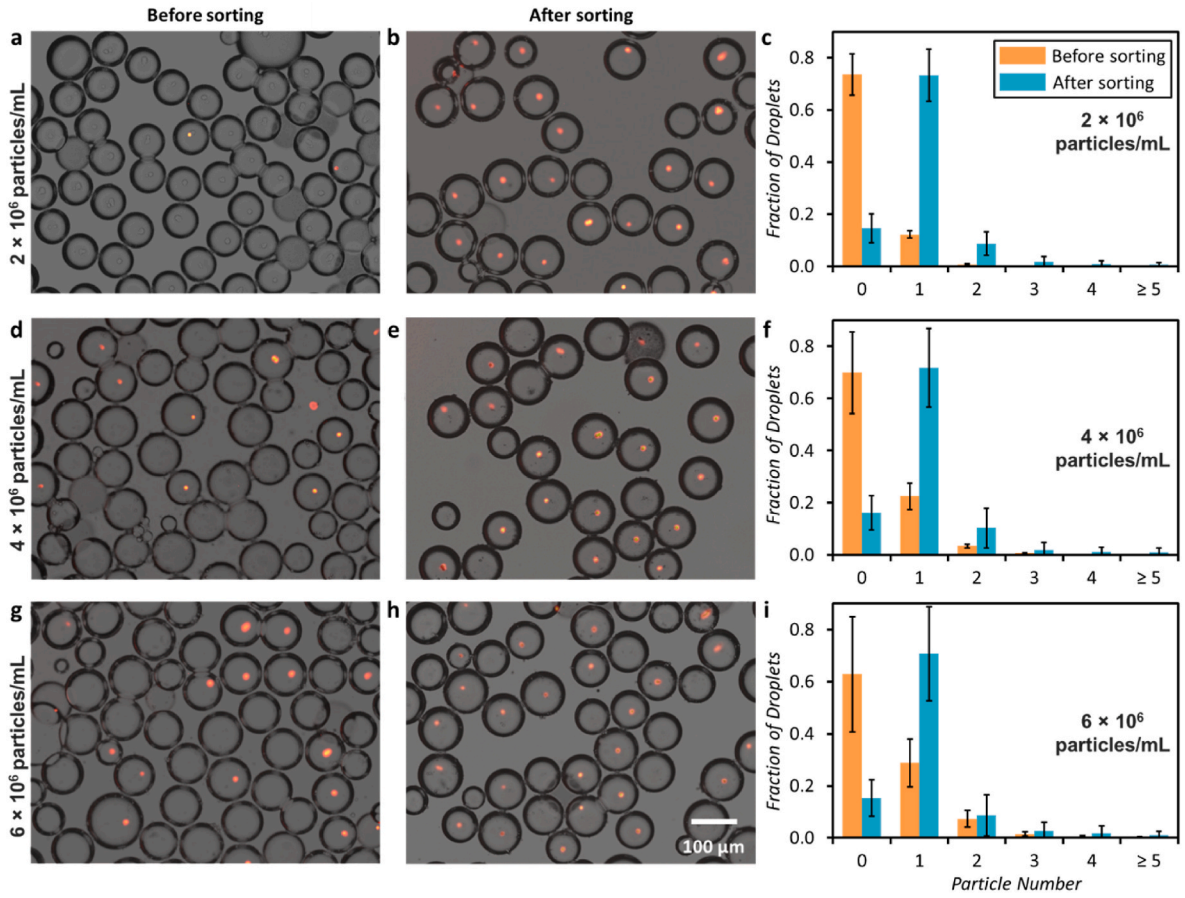


**Fig. 4.** Analysis of the single-bead encapsulation performance of the FAM-DSP system. Optical images and quantitative analysis for droplets' single-bead encapsulation performance without and with the application of the FAM-DSP system at bead concentrations of a-c) $2 \times 10^6$, d-f) $4 \times 10^6$, and g-i) $6 \times 10^6$ particles/mL.

and after using the FAM-DSP system, and Fig. 4a–h visually demonstrate this improvement. We examined the system using microbeads of three different concentrations: $2 \times 10^6$, $4 \times 10^6$, and $6 \times 10^6$ beads/mL. Without the detection and on-demand encapsulation processes, the majority of the droplets are empty or contain multiple beads, reflecting the random distribution predicted by the Poisson model. In contrast, the application of the FAM-DSP system leads to a much higher frequency of droplets containing the desired single bead, demonstrating the efficacy of our system in overcoming the limitations imposed by Poisson distribution predictions.

The bar charts given in Fig. 4c–f, and i quantitatively confirm the reduction in empty droplets and the improved encapsulation efficiency, with a notable increase in the number of droplets containing single beads across all concentrations. After using the FAM-DSP system for sorting and encapsulation, the single bead-laden droplet fraction increases from below 20% to over 70%, and the proportion of empty droplets is reduced to ~18%. While the number of empty droplets is significantly reduced, they are not fully eliminated. This is likely due to the inconsistent delay time required for the bead to travel to the capillary tip, caused by flow rate fluctuations due to the mechanical movement of the capillary tip. To solve this problem, future efforts will focus on refining the synchronization between the actuator and the fluorescence detection system and assessing system performance under diverse conditions, such as higher throughput and variable fluid viscosities, to minimize delay-induced variability. Despite the imperfection, the on-demand bead encapsulation demonstrates significant advantages over traditional methods, providing a more efficient approach for applications requiring single-target encapsulation.

The FAM-DSP system demonstrates several advantages over other recently developed systems for on-demand droplet sorting. Dielectrophoretic platforms, such as the high-definition single-cell printing system, achieve high sorting accuracy (>99.5%) and fast operation (up to 1 kHz) but require complex electrode setups and vacuum-based waste removal mechanisms (Zhang and Abate, 2020). Similarly, air-assisted systems produce highly uniform droplets (polydispersity index ~0.01%) but rely on high-pressure air streams and precise wettability modifications (Zhang et al., 2021). In contrast, the FAM-DSP system conducts sorting before encapsulation, achieving a reasonably high single-bead encapsulation efficiency and droplet uniformity while maintaining lower operational complexity and cost. This balance of simplicity, efficiency, and throughput makes the FAM-DSP system more suited for portable systems, where reducing complexity and cost is critical.

The simplicity and efficiency of the FAM-DSP system make it suitable for applications requiring continuous monitoring and analysis of single targets in a flow. We conducted ddELISA to demonstrate the capability of the FAM-DSP system. Currently, a significant challenge with ddELISA is the presence of a large number of empty droplets, which fill microscopy images with unnecessary information, reducing throughput and complicating the analysis. By minimizing the occurrence of empty droplets, we expect to allow microscopy images to contain more useful data, thereby streamlining the analysis process and improving the overall efficiency of the assay. To examine this, we adapt the workflow given in Fig. 5 for ddELISA using the FAM-DSP system.

Fig. 5a provides a detailed visual representation of the initial steps in the ddELISA workflow. Target antigen IFN-γ is first mixed with capture antibody-coated paramagnetic-fluorescent microbeads. These antigens bind to the capture antibodies on the beads, forming antibody-antigen complexes. Biotinylated detection antibodies and SβG are then added to the mixture, resulting in enzyme-labelled immunocomplexes. The

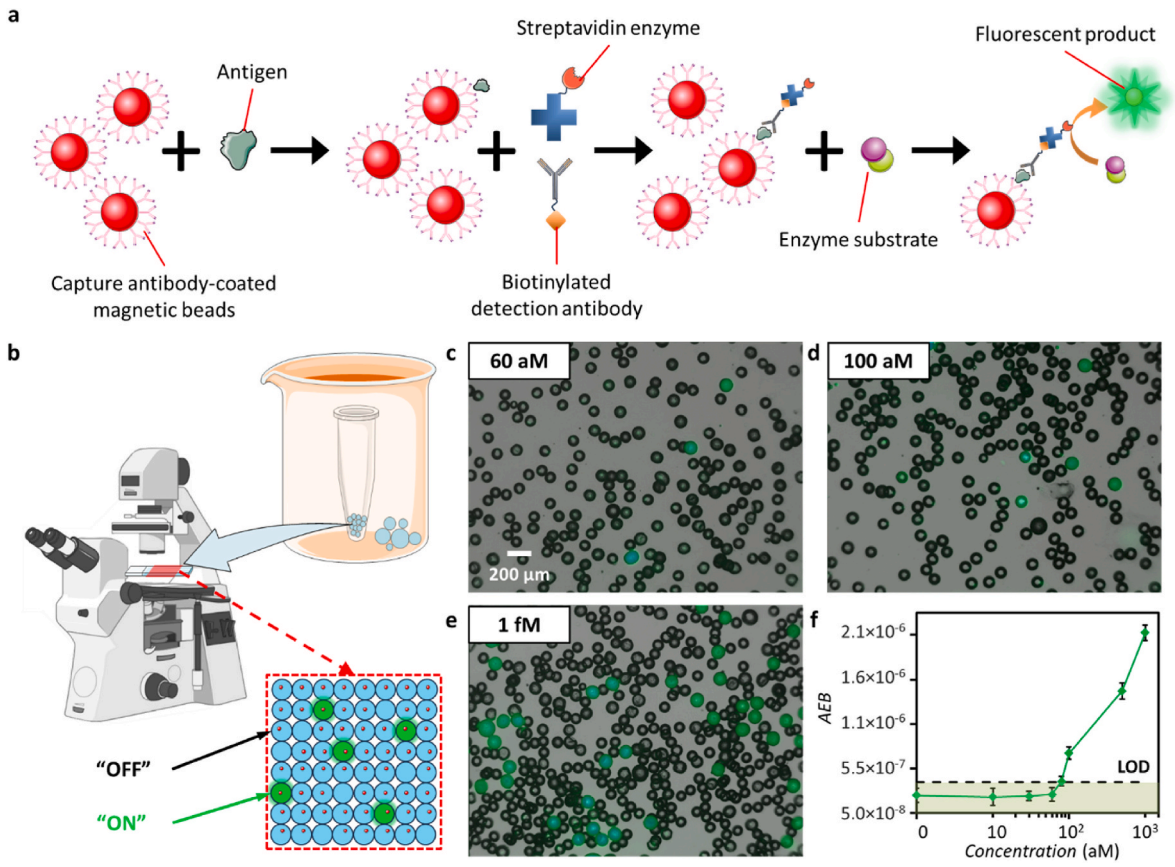


**Fig. 5.** Ultrasensitive biomarker detection using improved ddELISA. a) Processes of the bead-based sandwich immunoassay. Antigen: IFN-γ; Streptavidin enzyme: Streptavidin-β-galactosidase (SβG); Substrate: fluorescein di-β-d-galactopyranoside (FDG). b) Schematics showing the detection procedure. The bead-based immunocomplex is encapsulated into microdroplets using the FAM-DSP system. Then, the microdroplets are loaded onto a glass slide for analysis. Fluorescent images are obtained to identify the "ON" and "OFF" droplets. Representative dual-channel microscope images obtained for samples with different IFN-γ concentrations of c) 60 aM, d) 100 aM and e) 1 fM. f) Calibration curve for ddELISA for IFN-γ, the LOD is 60 aM.

immunocomplexes are mixed with an FDG fluorogenic substrate and then encapsulated into droplets using the FAM-DSP system. As illustrated in Fig. 5b, the subsequent steps involve loading the collected droplets onto a glass slide for imaging. A fluorescence microscope is used to identify and count the "ON" droplets that exhibit fluorescence, indicating the presence of the target IFN-γ protein. The ratio of "ON" droplets is a key concept in dELISA. The "ON" droplets contain at least one target protein molecule, while the "OFF" droplets contain none. By analysing the ratio of "ON" droplets, we can determine the average enzymes per bead (AEB), which provides a quantitative measure of the target protein concentration.

Our platform's ability to reduce the number of empty droplets significantly enhances the throughput and reliability of ddELISA. This reduction ensures that microscopy images contain more useful data, making the analysis process more efficient and improving the overall assay performance. The representative visual data given in Fig. 5c–e shows dual-channel microscope images of "ON" and "OFF" droplets at different concentrations (60 aM, 100 aM, and 1 fM). These dual-channel images highlight the high proportion of single-particle-containing droplets achieved using the FAM-DSP system (see Fig. S6 for the case without using the system), significantly reducing the occurrence of empty droplets and thereby facilitating more accurate quantification of target proteins. The calibration curve for IFN-γ detection, as depicted in Fig. 5f, demonstrates that the FAM-DSP system can lead to a low limit of detection (LOD) of ~60 aM. Our results show that LODs are similar for both on-chip and off-chip methods, indicating that the sorting process does not introduce additional systematic errors in ddELISA. The FAM-DSP system effectively balances simplicity and efficiency, significantly enhancing detection throughput without sacrificing operational accessibility. While the throughput of the FAM-DSP system, measured in the number of droplets detected per second, appears lower than that of advanced on-chip systems, it achieves a comparable liquid volume per second throughput, matching the performance of state-of-the-art on-chip platforms (Cohen et al., 2020; Yi et al., 2022). Also, a LOD of 60 aM is comparable to on-chip platforms. Importantly, this is accomplished without requiring cleanroom fabrication or complex fluidic controls, making the system both cost-effective and practical for routine applications.

Our results also indicate that the size variability (CV < 7%) for microdroplets obtained using the off-chip system is sufficient for the ddELISA application. In ddELISA, the low concentration of the biomarker ensures that each microbead captures less than one marker on average. As a result, the presence of a fluorescent signal in a droplet directly indicates the existence of the marker. Since the fluorescent signal intensity depends on the presence or absence of the biomarker rather than the exact droplet size, this level of size variability does not affect the performance or reliability of signal detection. While the FAM-DSP system demonstrated stable performance under controlled laboratory conditions, these factors may pose challenges in more variable environments. Future work will focus on assessing the system's robustness under fluctuating environmental conditions and with diverse fluid properties to ensure broad applicability.

## 4. Conclusion

In summary, we developed a versatile off-chip droplet production

platform capable of on-demand, single-target encapsulation. The core of the platform is an integrated fluorescent-activated mechanical droplet sorting and production (FAM-DSP) system. The FAM-DSP system is compact and low-cost, integrating both sorting and droplet production functionalities. The platform can precisely control droplet size, producing relatively uniformly sized microdroplets with diameters ranging from tens to hundreds of microns. Unlike conventional microchip-based approaches, the operation of our platform is simple and straightforward, significantly reducing equipment requirements for droplet generation and sorting. The capability of fluorescent-activated detection and mechanical droplet production and sorting allows for precise single-target encapsulation, achieving a high efficiency of above 70%, which is essential for applications requiring high specificity and reliability. We demonstrated the effectiveness of our platform in ddELISA for ultrasensitive biomarker detection. The use of the FAM-DSP system significantly reduces the number of empty droplets, thereby enhancing throughput and reliability. We envisage that our platform will be particularly advantageous for a wide range of applications, from routine clinical diagnostics to cutting-edge research in biomarker discovery, single-cell analysis, and disease monitoring. Future work will focus on further optimizing the platform's performance in terms of single-target encapsulation, droplet stability, system automation, and integration. Due to the relatively large size of the droplets produced in this study and the slower production rate compared to the on-chip system (Cohen et al., 2020), further optimization is needed to enhance throughput by reducing droplet size and increasing the production rate.

## CRediT authorship contribution statement

**Yuxin Zhang:** Writing – original draft, Data curation, Conceptualization. **Jiahao Zheng:** Investigation, Data curation. **Bayinqiaoge:** Investigation, Formal analysis, Investigation, Formal analysis. **Tim Cole:** Validation, Investigation. **Chengchen Zhang:** Supervision, Resources, Methodology, Data curation, Funding acquisition. **Yi Wang:** Supervision, Resources, Funding acquisition. **Shi-Yang Tang:** Writing – review & editing, Supervision, Resources, Project administration, Formal analysis, Conceptualization, Funding acquisition.

## Declaration of competing interest

The authors declare that they have no known competing financial interests or personal relationships that could have appeared to influence the work reported in this paper.

## Acknowledgements

S.-Y.T. gratefully acknowledges the research funded by the Australian Research Council Future Fellowship (FT230100257) and Discovery Project (DP250103029). C.Z. acknowledges the funding support from the Royal Society, UK (Grant Nos. RG/R1/241228 and IEC/NSFC/233339).

## Appendix A. Supplementary data

Supplementary data to this article can be found online at https://doi.org/10.1016/j.bios.2025.117134.

## Data availability

Data will be made available on request.

## References

Cohen, L., Walt, D.R., 2017. Single-molecule arrays for protein and nucleic acid analysis. Annu. Rev. Anal. Chem. 10 (1), 345–363.
Cohen, L., Cui, N., Cai, Y., Garden, P.M., Li, X., Weitz, D.A., Walt, D.R., 2020. Single molecule protein detection with attomolar sensitivity using droplet digital enzyme-linked immunosorbent assay. ACS Nano 14 (8), 9491–9501.
Cole, R.H., Tang, S.-Y., Siltanen, C.A., Shahi, P., Zhang, J.Q., Poust, S., Gartner, Z.J., Abate, A.R., 2017. Printed droplet microfluidics for on demand dispensing of picoliter droplets and cells. Proc. Natl. Acad. Sci. U.S.A. 114 (33), 8728–8733.
Collins, D.J., Neild, A., deMello, A., Liu, A.-Q., Ai, Y., 2015. The Poisson distribution and beyond: methods for microfluidic droplet production and single cell encapsulation. Lab Chip 15 (17), 3439–3459.
Guan, Z., Zou, Y., Zhang, M., Lv, J., Shen, H., Yang, P., Zhang, H., Zhu, Z., James Yang, C., 2014. A highly parallel microfluidic droplet method enabling single-molecule counting for digital enzyme detection. Biomicrofluidics 8 (1), 014110.
Joensson, H.N., Andersson Svahn, H., 2012. Droplet microfluidics—a tool for single-cell analysis. Angew. Chem. Int. Ed. 51 (49), 12176–12192.
Kaminski, T.S., Scheler, O., Garstecki, P., 2016. Droplet microfluidics for microbiology: techniques, applications and challenges. Lab Chip 16 (12), 2168–2187.
Kaushik, A.M., Hsieh, K., Wang, T.-H., 2018. Droplet microfluidics for high-sensitivity and high-throughput detection and screening of disease biomarkers. WIREs Nanomedicine and Nanobiotechnology 10 (6), e1522.
Liu, H., Li, M., Wang, Y., Piper, J., Jiang, L., 2020. Improving single-cell encapsulation efficiency and reliability through neutral buoyancy of suspension. Micromachines 11 (1), 94.
Mazutis, L., Gilbert, J., Ung, W.L., Weitz, D.A., Griffiths, A.D., Heyman, J.A., 2013. Single-cell analysis and sorting using droplet-based microfluidics. Nat. Protoc. 8 (5), 870–891.
Moragues, T., Arguijo, D., Beneyton, T., Modavi, C., Simutis, K., Abate, A.R., Baret, J.-C., deMello, A.J., Densmore, D., Griffiths, A.D., 2023. Droplet-based microfluidics. Nature Reviews Methods Primers 3 (1), 32.
Nielsen, J.B., Hanson, R.L., Almughamsi, H.M., Pang, C., Fish, T.R., Woolley, A.T., 2020. Microfluidics: innovations in materials and their fabrication and functionalization. Anal. Chem. 92 (1), 150–168.
Sánchez Barea, J., Lee, J., Kang, D.-K., 2019. Recent advances in droplet-based microfluidic Technologies for biochemistry and molecular biology. Micromachines 10 (6), 412.
Shim, J.-u., Ranasinghe, R.T., Smith, C.A., Ibrahim, S.M., Hollfelder, F., Huck, W.T.S., Klenerman, D., Abell, C., 2013. Ultrarapid generation of femtoliter microfluidic droplets for single-molecule-counting immunoassays. ACS Nano 7 (7), 5955–5964.
Tang, S.-Y., Wang, K., Fan, K., Feng, Z., Zhang, Y., Zhao, Q., Yun, G., Yuan, D., Jiang, L., Li, M., Li, W., 2019. High-throughput, off-chip microdroplet generator enabled by a spinning conical frustum. Anal. Chem. 91 (5), 3725–3732.
Ye, S., Li, C., Zheng, X., Huang, W., Tao, Y., Yu, Y., Yang, L., Lan, Y., Ma, L., Bian, S., Du, W., 2022. OsciDrop: a versatile deterministic droplet generator. Anal. Chem. 94 (6), 2918–2925.
Yelleswarapu, V., Buser, J.R., Haber, M., Baron, J., Inapuri, E., Issadore, D., 2019. Mobile platform for rapid sub–picogram-per-milliliter, multiplexed, digital droplet detection of proteins. Proc. Natl. Acad. Sci. USA 116 (10), 4489–4495.
Yi, J., Gao, Z., Guo, Q., Wu, Y., Sun, T., Wang, Y., Zhou, H., Gu, H., Zhao, J., Xu, H., 2022. Multiplexed digital ELISA in picoliter droplets based on enzyme signal amplification block and precisely decoding strategy: a universal and practical biodetection platform. Sensor. Actuator. B Chem. 369, 132214.
Yue, X., Fang, X., Sun, T., Yi, J., Kuang, X., Guo, Q., Wang, Y., Gu, H., Xu, H., 2022. Breaking through the Poisson Distribution: a compact high-efficiency droplet microfluidic system for single-bead encapsulation and digital immunoassay detection. Biosens. Bioelectron. 211, 114384.
Zhang, P., Abate, A.R., 2020. High-definition single-cell printing: cell-by-cell fabrication of biological structures. Adv. Mater. 32 (52), 2005346.
Zhang, Y., Zhao, Q., Yuan, D., Liu, H., Yun, G., Lu, H., Li, M., Guo, J., Li, W., Tang, S.-Y., 2020. Modular off-chip emulsion generator enabled by a revolving needle. Lab Chip 20 (24), 4592–4599.
Zhang, P., Chang, K.-C., Abate, A.R., 2021. Precision ejection of microfluidic droplets into air with a superhydrophobic outlet. Lab Chip 21 (8), 1484–1491.
Zhang, P., Xu, L., Chen, H., Abate, A.R., 2023. Flow cytometric printing of double emulsions into open droplet arrays. Lab Chip 23 (10), 2371–2377.
Zheng, Y., Wu, Z., Hou, Y., Li, N., Zhang, Q., Lin, J.-M., 2023. Microfluidic engineering of crater–terrain hydrogel microparticles: toward novel cell carriers. ACS Appl. Mater. Interfaces 15 (6), 7833–7840.
Zhu, Z., Chen, T., Huang, F., Wang, S., Zhu, P., Xu, R.X., Si, T., 2024. Free-boundary microfluidic platform for advanced materials manufacturing and applications. Adv. Mater. 36 (7), 2304840.